# Supplementary Material for "Dynamically tunable lamellar surface structures from magnetoactive elastomers driven by a uniform magnetic field"

Izidor Straus,[1] Gašper Kokot,[2] Gaia Kravanja,[3] Luka Hribar,[3] Raphael Kriegl,[4] Mikhail Shamonin,[4] Matija Jezeršek,[3] and Irena Drevenšek-Olenik[1,2]

[1] *University of Ljubljana, Faculty of Mathematics and Physics, Ljubljana, Slovenia.*
[2] *Jožef Stefan Institute, Ljubljana, Slovenia.*
[3] *University of Ljubljana, Faculty of Mechanical Engineering, Ljubljana, Slovenia.*
[4] *Ostbayerische Technische Hochschule Regensburg, Regensburg, Germany.*

(Dated: April 4, 2023)

## ADDTIONAL EXAMPLES OF THE RELATIVE REFLECTANCE RELAXATION CURVES FOR STRETCHING AND STICKING REGIMES

This section complements an example of the relaxation process for the *deflecting* regime presented in Fig. 4 bottom. Fig. S1 left, shows the *stretching* regime, and Fig. S1 right, the *sticking* regime.

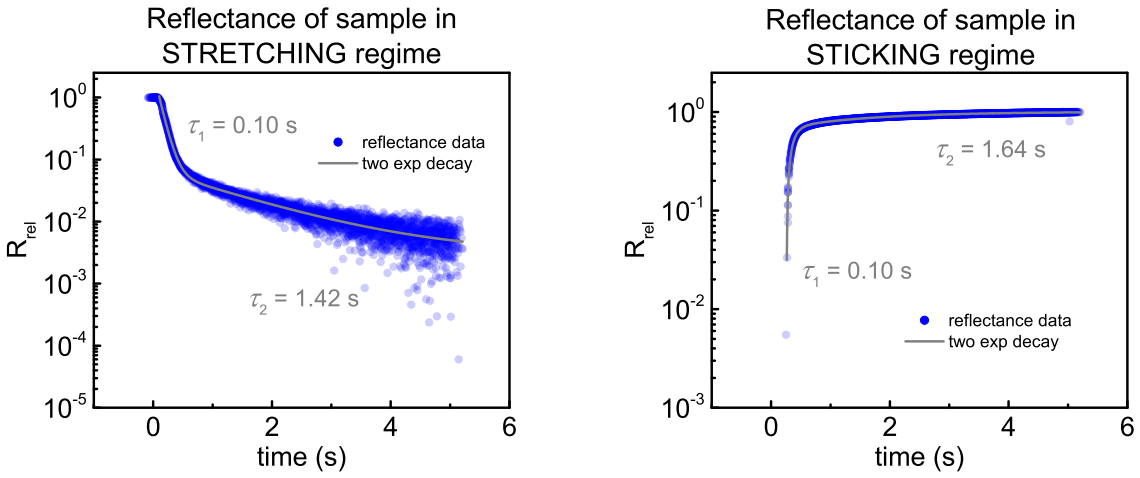


Fig. S1. **Left**: an example of the relaxation process of a single lamella for a sample in the *stretching* regime, when the field is switched off. Data points represent the time relaxation of $R_{rel}$ for 10 consecutive off pulses. A two exponential decay is fitted to the measurement and two relaxation times are extracted from the fit (short $\tau_1$ and long $\tau_2$). In order to determine characteristic relaxation times for the whole sample. this analysis is averaged over several lamellae. **Right**: an example of the two exponential relaxation analysis for a sample from the *sticking* regime. For samples in this regime, the relative reflectance $R_{rel}$ rises when the magnetic field is switched off and falls when the magnetic field is switched on. This is a reversed situation compared to the *stretching* and *deflecting* regimes. We explain this by acknowledging, that only small bending occurs before lamellae sticking begins, not allowing light to deflect from the sides of lamella as described in the main text (Fig. 5). However, small deflection is still sufficient to cover the dips between lamellae, which typically reflect more light as a result of the ablation process. Direct laser micromachining exposes CIP particles in the polymer to the surface, allowing for larger light reflection. Both of these processes help to explain why in sticking regime $R_{rel}$ rises when lamellae relax to their straight position.

## CONTINUUM MECHANICS MODEL FOR LARGE DEFLECTIONS WHEN A COMBINATION OF BENDING AND BUCKLING POINT FORCES ARE ACTING ON AN EULER-BERNOULLI BEAM

### General solution

In our endavour to model large deflections of a magnetoactive elastomer (MAE) lamella we have followed reference [1]. Because that reference is not peer reviewed, we repeat here the derivation for our specific need and add the details on calculation of the coefficients that enter the solution scheme. In brief, the calculation procedure performs the following: We slice the cantilever into equidistant pieces. Next we calculate all the forces (gravity and magnetic

dipolar forces acting on the particles) native to a particular slice. After that the total force acting on each slice, because the total force is what ultimately determines the deflection. To calculate the deflection of each slice we use the general solution we derive below.

In this SI document we will adopt the same geometry and lamella orientation as in [1] in order to make the comparison easier and because this is how it is implemented in the algorithm. The reason to choose to align the cantilever along $x$ is calculational convenience to avoid infinite or close to infinite derivative conditions. The reader should note that compared to the main text of this article this means the $x$ and $y$ coordinates here are switched. The cantilever has the base at $x = L$ and the tip at $x = 0$ (see Fig. S2), we assume the deflection in the $y$ direction. As this is the first step in elucidating the influence of neighbouring lamellae on the deflection, Young's modulus $E$ is assumed constant, eventhogh it is known it can drastically increase when MAE is subjected to an external magnetic field, yet no mathematical model exists for the functional dependence of $E$ on magnetic flux density $B$. The second moment of area $I$ for a rectangular cross-section (our case) is constant along $x$. This enables us to write the primary differential equation for the deflection in Euler-Bernoulli beam theory, which we aim to solve:

$$\frac{y''}{(1+(y')^2)^{3/2}} = \frac{M(x,y)}{EI} = \Xi(x,y) = \alpha x + \beta y, \tag{1}$$

where the $'$ denotes derivative with respect to $x$ and $M(x,y)$ is the total torque. This is a non-linear version of the more common approximation for small deflections: $\dot{y} = 0$. The solution to Eq. 1 for forces acting in both $x$ and $y$ direction begins with the ansatz $\Xi(x,y) = \alpha x + \beta y$. In this ansatz it is already assumed that we only have forces acting on the Euler-Bernoulli beam and that these forces produce a torque with the levers being the $x$ and $y$. We do not include any explicit torques therefore we refer the reader to Eq. 34.1 in [1] for a demonstration on how to implement explicit torques through intermittent translations specific to each slice which enables to use the solutions to Eq. 1 that we will outline now.

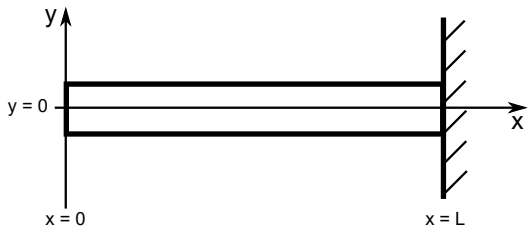


Fig. S2. A sketch of the cantilever orientation.

We are solving the differental equation:

$$\frac{y''}{(1+(y')^2)^{3/2}} = \alpha x + \beta y. \tag{2}$$

We will introduce new variables twice, chosen in a way that Eq. 2 becomes analitically manageable. The first set of new variables $u$ and $v$ is:

$$\begin{aligned} u &= \frac{\alpha}{\sqrt{\alpha^2+\beta^2}}x + \frac{\beta}{\sqrt{\alpha^2+\beta^2}}y, \\ v &= \frac{\alpha}{\sqrt{\alpha^2+\beta^2}}x - \frac{\beta}{\sqrt{\alpha^2+\beta^2}}y, \end{aligned} \tag{3}$$

which implies $\alpha x + \beta y = \sqrt{\alpha^2+\beta^2}u$. Note that, if $\alpha = 0$ then $u = -v = y$ or if $\beta = 0$ then $u = v = x$, this transformation becomes pointless, which underscores the importance of the problem at hand to truly have both $x$ and

$y$ components of the force. Calculating the derivatives needed to insert into Eq. 2 from manipulation of Eqs. 3 yields:

$$\begin{aligned}
\frac{\mathrm{d}x}{\mathrm{du}} &= \dot{x} = \frac{\sqrt{\alpha^2+\beta^2}}{2\alpha}(1+\dot{v}),\\
\frac{\mathrm{d}y}{\mathrm{du}} &= \dot{y} = \frac{\sqrt{\alpha^2+\beta^2}}{2\beta}(1-\dot{v}),\\
\frac{\mathrm{d}y}{\mathrm{dx}} &= y' = \frac{\alpha}{\beta}\frac{(1-\dot{v})}{(1+\dot{v})},\\
\frac{\mathrm{d}^2y}{\mathrm{dx}^2} &= y'' = -\frac{4\alpha^2}{\beta\sqrt{\alpha^2+\beta^2}}\frac{\ddot{v}}{(1+\dot{v})^3},
\end{aligned} \tag{4}$$

where we use the dot notation to denote a derivative with respect to $u$. Left side of Eq. 2 becomes:

$$\frac{y''}{(1+(y')^2)^{3/2}} = -\frac{4\alpha^2\beta^2}{(\alpha^2+\beta^2)^2}\frac{\ddot{v}}{\left[\left(\dot{v}+\frac{\beta^2-\alpha^2}{\beta^2+\alpha^2}\right)^2+1-\left(\frac{\beta^2-\alpha^2}{\beta^2+\alpha^2}\right)^2\right]^{3/2}}. \tag{5}$$

We introduce another variable $\theta$ such that:

$$\begin{aligned}
\dot{v}+\frac{\beta^2-\alpha^2}{\beta^2+\alpha^2} &= \sqrt{1-\left(\frac{\beta^2-\alpha^2}{\beta^2+\alpha^2}\right)^2}\tan\theta\\
\ddot{v} &= \sqrt{1-\left(\frac{\beta^2-\alpha^2}{\beta^2+\alpha^2}\right)^2}(1+\tan^2\theta)\dot{\theta}.
\end{aligned} \tag{6}$$

We insert Eqs. 6 into Eq. 5:

$$\frac{y''}{(1+(y')^2)^{3/2}} = -\frac{\dot{\theta}}{\sqrt{1+\tan^2\theta}} \tag{7}$$

which together with Eq. 2 and $\alpha x+\beta y = \sqrt{\alpha^2+\beta^2}u$ means:

$$\frac{\dot{\theta}}{\sqrt{1+\tan^2\theta}} = \pm\dot{\theta}\cos\theta = -\sqrt{\alpha^2+\beta^2}u \tag{8}$$

and upon integration:

$$\begin{aligned}
\pm\sin\theta &= -\int\sqrt{\alpha^2+\beta^2}u\,\mathrm{du}+C_1,\\
\cos\theta &= \pm\sqrt{1-\left(-\int\sqrt{\alpha^2+\beta^2}u\,\mathrm{du}+C_1\right)^2}
\end{aligned} \tag{9}$$

with $C_1$ being an integration constant. Inserting Eqs. 9 back into the first equation of Eqs. 6 and substituting $\tan\theta = \frac{\sin\theta}{\cos\theta}$ yields:

$$\begin{aligned}
\dot{v} &= \pm\sqrt{1-\left(\frac{\beta^2-\alpha^2}{\beta^2+\alpha^2}\right)^2}\frac{-\int\sqrt{\alpha^2+\beta^2}u\,\mathrm{du}+C1}{\sqrt{1-\left(-\int\sqrt{\alpha^2+\beta^2}u\,\mathrm{du}+C1\right)^2}}+\frac{\alpha^2-\beta^2}{\beta^2+\alpha^2} =\\
&= \pm\sqrt{1-\left(\frac{\beta^2-\alpha^2}{\beta^2+\alpha^2}\right)^2}\frac{-\sqrt{\alpha^2+\beta^2}\frac{u^2}{2}+C1}{\sqrt{1-\left(-\sqrt{\alpha^2+\beta^2}\frac{u^2}{2}+C1\right)^2}}+\frac{\alpha^2-\beta^2}{\beta^2+\alpha^2}
\end{aligned} \tag{10}$$

and after another integration:

$$v = \pm\sqrt{1-\left(\frac{\beta^2-\alpha^2}{\beta^2+\alpha^2}\right)^2}\int\frac{-\sqrt{\alpha^2+\beta^2}\frac{u^2}{2}+C1}{\sqrt{1-\left(-\sqrt{\alpha^2+\beta^2}\frac{u^2}{2}+C1\right)^2}}\,\mathrm{du}+\frac{\alpha^2-\beta^2}{\beta^2+\alpha^2}u+C2. \tag{11}$$

Now that we are equipped with Eqs. 10 and 11 we can numerically determine $C1$ and $C2$ for each slice by introducing the correct boundary conditions between slices.

### Determining parameters $\alpha$ and $\beta$

We now move from the general solution of Eq. 2 to implementing the solution in a sliced cantilever. Refer to Table I before reading further. We choose the number of slices $N_{slices}$ we would like to have and make equidistant slices of

| | | |
|---|---|---|
| lamella height | $L = 300\,\mu\text{m}$ | Marked $h$ in the main text Fig. 1. |
| lamella base width | $b = 70\,\mu\text{m}$ | Marked $w$ in the main text Fig. 1. |
| lamella base length | $l = 30\,\mu\text{m}$ | Marked $l$ in the main text Fig. 1. We do not take the full lamella length because we are interested how a narrow section of lamella interacts with the neighbouring lamella. This empowers us to make conclusions about the frustration of long lamellar structures. |
| lamella total volume | $V = 6.3 \cdot 10^{-13}\,\text{m}^3$ | $V = Lbl$ |
| second moment of area | $I = 8.575 \cdot 10^{-17}\,\text{m}^4$ | Rectangular base, rotation along the $l$ direction, $I = \frac{b^3 l}{12}$. |
| elastomer density | $\rho_E = 0.965\,\text{g cm}^{-3}$ | Material is polydimethylsiloxane (PDMS). |
| elastomer Youngs' modulus | $E_0 = 45\,\text{kPa}$ | A typical value for MAE. |
| particle density | $\rho_P = 7.874\,\text{g cm}^{-3}$ | Material is iron. |
| particle radius | $r_P = 2.25\,\mu\text{m}$ | We make the simplification of a fixed particle radius instead of a particular distribution. |
| particle percentage by mass (weight percentage) in MAE | $w_w = 75\,\text{wt\%}$ | |
| single particle volume | $V_{P1} = 4.771 \cdot 10^{-17}\,\text{m}^3$ | $V_{P1} = \frac{4}{3}\pi r_P^3$ |
| single particle mass | $m_{P1} = 3.757 \cdot 10^{-13}\,\text{kg}$ | $m_{P1} = \rho_P V_{P1}$ |
| number of particles | $N_P = 3549$ | $N_P = \frac{w_w \rho_E V}{(\rho_P - w_w(\rho_P - \rho_E))V_{P1}}$, derived from $w_w$ definition $w_w = \frac{N_P m_{P1}}{N_P m_{P1} + \rho_E (V - N_P V_{P1})}$. |
| volume of all particles inside lamella | $V_P = 1.693 \cdot 10^{-13}\,\text{m}^3$ | $V_P = N_P V_{P1}$ |
| particle percentage by volume | $w_V = 26.88\,\text{V\%}$ | $w_V = \frac{V_P}{V}$ |
| lamella total mass | $m = 1.778 \cdot 10^{-9}\,\text{kg}$ | $m = \rho_P V_P + \rho_E (V - V_P)$ |
| gravitational constant | $g = 9.81\,\text{m s}^{-2}$ | |
| vacuum magnetic permeability | $\mu_0 = 4\pi \cdot 10^{-7}\,\text{H m}^{-1}$ | |
| | $\frac{mg}{E_0 I} = 2 \cdot 10^4\ \text{m}^{-2}$ | The contribution to the deflecting parameter $\alpha$ coming from gravity. |
| | $\frac{\mu_0 m_n^2}{E_0 I} = 10^{-17}\ \text{m}^2$ | The amplitude of the contribution to both deflecting parameters $\alpha$ and $\beta$ coming from magnetic dipolar forces. The values that enter $\alpha$ and $\beta$ also depend on the distance between particles belonging to different (neighboring) lamellae (see Eq. 12). In the next step of the development of this model, the induced magnetic moment $m_n$ at specific $B$ should be calculated from the magnetization curve. This step should be performed together with: (1) taking into account demagnetizing factors, and (2) implementation of $E_0$ dependance on $B$. Both were neglected at this initial point of the development of the model as they deserve a separate dedicated investigation. This is why we do not to speculate on any $B$ dependance at this point. Nevertheless a qualitative explanation of the observed lamellar frustration is still possible as well as pitch functional dependence and the effect of different random particle configurations can be explained. |
| | $\frac{\mu_0 m_n^2}{E_0 I p^4} = 0.02\ \text{m}^{-2}$ | The amplitude of the contribution to both deflecting parameters $\alpha$ and $\beta$ coming from the magnetic dipolar force, additionally normalized by the distance between the neighbouring lamellae, i.e. pitch $p = 150\ \mu$m used in calculations for the histogram in Fig. 2d. Note that this is for one pair of particles only and for the final dipolar force we still sum over all the pairs between the particle inside the deflecting lamela and the neighbourhood, and then over all particles within the slice. |

TABLE I. Parameters used in the simulation with comments.

length $L_i = L/N_{slices}$, where $i$ denotes the $i$-th slice. The force native to each slice comes from two sources. One is gravity according to our cantilever orientation $\vec{F_{gi}} = (m_i g, 0)$, where $m_i$ is the mass of each slice determined from $m_i = m/N_{slices}$. In our case this force only has $x$ component and only contributes to $\alpha$ with $\frac{m_i g}{E_0 I}$. The second force source is the magnetic dipolar force between two particles, which for convenience we write slightly differently than in the main text in order to highlight the parameter from Table I entering $\alpha$ and $\beta$:

$$\frac{\vec{F}_{md}}{E_0 I} = \frac{\mu_0 m_n^2}{E_0 I}\frac{3}{4\pi r^5}\left(\left(\frac{\vec{m}_i}{m_n}\cdot\vec{r}\right)\frac{\vec{m}_j}{m_n} + \left(\frac{\vec{m}_j}{m_n}\cdot\vec{r}\right)\frac{\vec{m}_i}{m_n} + \vec{r} - \frac{5\left(\frac{\vec{m}_j}{m_n}\cdot\vec{r}\right)\left(\frac{\vec{m}_i}{m_n}\cdot\vec{r}\right)}{r^2}\vec{r}\right), \tag{12}$$

where we already assumed that magnetic moment is only induced along $B$ direction and that the magnitude $m_n$ is the same for $\vec{m}_i$ particles inside the deflecting lamella slice $i$ and for $\vec{m}_j$ particles inside the neighbouring lamella/e (all of them, we do not slice the neighbourhood). This would be true when particles are saturated. The contribution of this force for each particle is summed over all neighbours, which in our simplification are only the particles from the neighbouring lamella/e and not the particles within the same lamella. Then the total magnetic dipolar force native to the slice is a sum of all the magnetic dipolar forces acting on individual particles within the slice. Here lies the essence of our analysis as each particle configuration is unique and the deflections form a histogram reported in Fig. 2d in the main text. It has components in $x$ and $y$ directions contributing to $\alpha$ and $\beta$ native to a specific slice. We use the phrase "force native to the slice" in order to point out a crucial technical detail. Once we have used the above procedure to collect and sum all the forces (all the dipolar magnetic forces and gravity) into a singular point force acting on the slice we need to ask, if this is the total force $\vec{F}_i$ acting on the slice $i$. In order to obtain $\vec{F}_i$ we now need to add to each force native to the slice in question also the forces native to the slices above it (above meaning away from the base) and thus obtain the final $\alpha$ and $\beta$ entering the algorithm. The reason for this is the easiest to imagine, if we consider for a moment gravity only. Each slice feels the weight of the part of the beam above but not below. $\alpha_i$ and $\beta_i$ will from this point onward refer to $\frac{\vec{F}_i}{E_0 I} = (\alpha_i, \beta_i)$.

### Implementing slice conditions

Each slice $i$ has to satisfy Eg. 2, where we write down the . At the boundary $i$ between two slices $i$ and $i-1$ the coordinates $x$ and $y$ must coincide to ensure continuity. This is coupled with the expectation of a smooth deflection without breaks in the slope of the deflected cantilever: $y'_{i-1}(x_i) = y'_i(x_i)$. Those two boundary conditions imply also $u_i(x_i, y_i) = u_{i-1}(x_i, y_i)$; $v_i(x_i, y_i) = v_{i-1}(x_i, y_i)$; and $\dot{v}_{i-1}(u_i) = \dot{v}_i(u_i)$.

Slice lengths $L_i$ are an input for our algorithm. We can express the slice $i$ length:

$$L_i = \sqrt{\Delta x_i^2 + \Delta y_i^2} = \Delta u_i \sqrt{\left(\frac{\Delta x_i}{\Delta u_i}\right)^2 + \left(\frac{\Delta y_i}{\Delta u_i}\right)^2} = \Delta u_i \sqrt{\left(\frac{\mathrm{d}x}{\mathrm{d}u}\right)^2 + \left(\frac{\mathrm{d}y}{\mathrm{d}u}\right)^2}, \tag{13}$$

where $\Delta u_i = u_{i+1} - u_i$ and from first and second line in Eq. 4:

$$L_i = (u_{i+1} - u_i)\frac{\sqrt{\alpha_i^2 + \beta_i^2}}{2}\sqrt{\left(\frac{1 + \dot{v}_i(u_i)}{\alpha_i}\right)^2 + \left(\frac{1 - \dot{v}_i(u_i)}{\beta_i}\right)^2}. \tag{14}$$

From above we can determine the slice $u_i$, by knowing the $L_i$, the next slice $u_{i+1}$, and $\dot{v}_{i+1}(u_i) = \dot{v}_i(u_i)$. The first step is to obtain the value of $\dot{v}_i$ from Eq. 10:

$$\dot{v}_i(u_i) = \pm\sqrt{1 - \left(\frac{\beta_i^2 - \alpha_i^2}{\beta_i^2 + \alpha_i^2}\right)^2}\frac{-\sqrt{\alpha_i^2 + \beta_i^2}\frac{u_i^2}{2} + C1_i}{\sqrt{1 - \left(-\sqrt{\alpha_i^2 + \beta_i^2}\frac{u_i^2}{2} + C1_i\right)^2}} + \frac{\alpha_i^2 - \beta_i^2}{\beta_i^2 + \alpha_i^2}. \tag{15}$$

Then we obtain $C1_i$ by imposing the boundary conditions, starting at the base $i = N_{slices} = n$. Because the beam stays attached perepndicular to the substrate at the base ($x_n = L$, $y_n = 0$) $y'_n(L) = 0$ as well as $u_n = \frac{\alpha_{n-1}}{\sqrt{\alpha_{n-1}^2 + \beta_{n-1}^2}}L$ and from the third line in Eq. 4 we get the condition that enables us to determine $C1_n$ :

$$\frac{\alpha_{n-1}}{\beta_{n-1}}\left(\frac{1 - \dot{v}_n(u_n)}{1 + \dot{v}_n(u_n)}\right) = \frac{\alpha_{n-1}}{\beta_{n-1}}\left(\frac{1 - \dot{v}_n\left(\frac{\alpha_{n-1}}{\sqrt{\alpha_{n-1}^2 + \beta_{n-1}^2}}L\right)}{1 + \dot{v}_n\left(\frac{\alpha_{n-1}}{\sqrt{\alpha_{n-1}^2 + \beta_{n-1}^2}}L\right)}\right) = 0, \tag{16}$$

which together with Eq. 10 offers $C1_n$. Now we can determine $C2_n$ because we know the outcome of the integration of Eq. 11:

$$v_n(u_n) = u_n = \frac{\alpha_{n-1}}{\sqrt{\alpha_{n-1}^2 + \beta_{n-1}^2}} L. \tag{17}$$

For the other slices $i$ we repeat these steps to determine each slice $u_i$, by knowing the $L_i$, the next slice $u_{i+1}$, and $\dot{v}_{i+1}(u_i) = \dot{v}_i(u_i)$ to employ condition Eq. 14. The second condition to determine each $C1_i$ is equivalent to Eq. 16:

$$\frac{\alpha_{i+1}}{\beta_{i+1}} \left( \frac{1 - \dot{v}_{i+1}(u_i)}{1 + \dot{v}_{i+1}(u_i)} \right) = \frac{\alpha_i}{\beta_i} \left( \frac{1 - \dot{v}_i(u_i)}{1 + \dot{v}_i(u_i)} \right). \tag{18}$$

Finally the condition $v_i(u_i) = v_{i+1}(u_i)$ and Eq. 11 determines all $C2_i$ and consequently via Eq. 11 also $v_i$ become known. Once we have all $u_i$ and $v_i$ we use Eq. 3 to obtain all $x_i$ and $y_i$.

[1] F. A. Chouery, Exact and numerical solutions for large deflection of elastic non-prismatic beams, FAC Systems INC., WA (2006).